Statistically Equivalent Representative Volume Elements for Unidirectional Composite Microstructures: Part I – Without Damage

SHRIRAM SWAMINATHAN,[1] SOMNATH GHOSH[1,*] AND N. J. PAGANO[1,2]
[1]*Department of Mechanical Engineering, The Ohio State University Columbus, OH 43202, USA*
[2]*AFRL/MLBC, Wright-Patterson AFB OH 45433-7750, USA*

(Received ...)

ABSTRACT: The representative volume element (RVE) of a material microstructure plays an important role in the analysis of heterogeneous materials, such as composites. Effective material properties in a composite material depend on the microstructural concentration and dispersion of different phases in the RVE. In this study, a combination of statistical and computational tools are proposed for identifying the statistically equivalent RVE (SERVE) for an elastic composite with nonuniform dispersion of inclusions. Numerical tests are conducted with various statistical functions of geometry, stresses, and strains to examine the validity of potential alternative definitions of the SERVE. In the first of this two-part article, methods are addressed for undamaged composite microstructures with continuous interfaces between the fiber and the matrix. The sequel article deals with the evolution of SERVE caused by damage due to interfacial debonding.

KEY WORDS: statistically equivalent representative volume element (SERVE), Voronoi cell FEM (VCFEM), marked correlation function, critical interfacial fraction.

INTRODUCTION

COMPOSITE MATERIALS HAVE gained wide commercial acceptance in recent times due to their superior thermal and mechanical properties like high strength and stiffness to weight ratio, thermal conductivity, etc. Effective macroscopic mechanical and thermal properties like stiffness and strength of these materials, depend not only on the properties of individual constituents but also on the local microstructural morphology. Typical morphological parameters of relevance include the fiber volume fraction, inclusion size

*Author to whom correspondence should be addressed. E-mail: ghosh.5@osu.edu

0021-9983/04/00 0001–22 $10.00/0 DOI: 10.1177/00219830?055273

and shape and orientation, the spatial dispersion of the fibers in the matrix, the state of the interface (e.g., bonded or debonded), etc. The effect of local morphology is even more pronounced on failure properties, such as fracture toughness and ductility. Effective properties are evaluated by methods of homogenization or averaging of microscopic variables like stresses and strains over a representative volume element (RVE) of the microstructure, which is an important parameter in the micromechanical analysis of composite materials. The concept of RVE was introduced by Hill in [1] as a microstructural sub-region that is representative of the entire microstructure in an average sense. Hashin and Shtrikman [2,3] extended the concept and introduced representative volume as a reference cube that is small compared to the entire body, for which the volume average of variables like strain, stress, or phase volume fraction are the same as those for the whole body. The stresses and strains in their analysis are derived using homogeneous boundary conditions [4], so that either the displacement on the cube surface, S, is prescribed according to $u_i(S) = \varepsilon^0_{ij} x_j$ or the tractions prescribed as $T_i(S) = \sigma^0_{ij} n_j$, where ε^0_{ij} and σ^0_{ij} are constants. Similar definitions of RVE have been given for example, in [5,6]. Willis [7] has proposed a two-point probability measure to get statistically equivalent RVEs (SERVEs) for composites with random variations in the microstructure. A number of studies have been conducted with the RVE, represented by a unit cell consisting of a single heterogeneity in a regular (square, cubic, hexagonal, etc.) matrix [8,9]. The underlying assumptions in these studies, are that the microstructures depict a uniform periodically repetitive array of heterogeneities and the body is subjected to homogeneous boundary conditions. A few efforts by, for example, Boehm et al. [10,11] have considered limited extensions of the unit cell models with creative boundary conditions to accommodate the effects of microstructural non-uniformities. In practice, however, the occurrence of perfect uniformity or periodicity are rare in composite microstructures. Even when geometric periodicity may be evident, periodicity in the evolution of microstructural variables, for example, in plasticity analysis or in problems with evolving damage is often in question. Unit cell assumptions in damage evolution imply that all the particles or interfaces are damaged simultaneously, which is far from reality in most cases. Failure-related predictions, e.g., strain-to-failure, fracture toughness, etc. have been rather poor in these models since they bear little relationship to the actual stereographic features.

While the RVE, according to the strictest definitions may be unattainable for microstructures with nonuniform dispersions, it is of significant interest to identify statistically equivalent RVEs (SERVEs) that may be used to evaluate accurate homogenized properties to be used in macroscopic analysis. In this sense, a SERVE can be identified as the smallest volume element of the microstructure exhibiting the following characteristics:

(i) The effective material properties, e.g., stress–strain behavior in the SERVE should be equivalent to the properties of the entire microstructure, at least locally to within a prescribed tolerance.
(ii) Distribution functions of parameters reflecting the local morphology, like local volume fraction, neighbor distance, or radial distributions, in the SERVE should be equivalent to those for the overall microstructure.
(iii) The SERVE chosen should be independent of the location in the local microstructure as well as of the applied loading direction, even for anisotropic material response.

In Figure 1(b), a circular region is used to identify N inclusions in the RVE. The heterogeneous domain containing these inclusions is then tessellated to construct

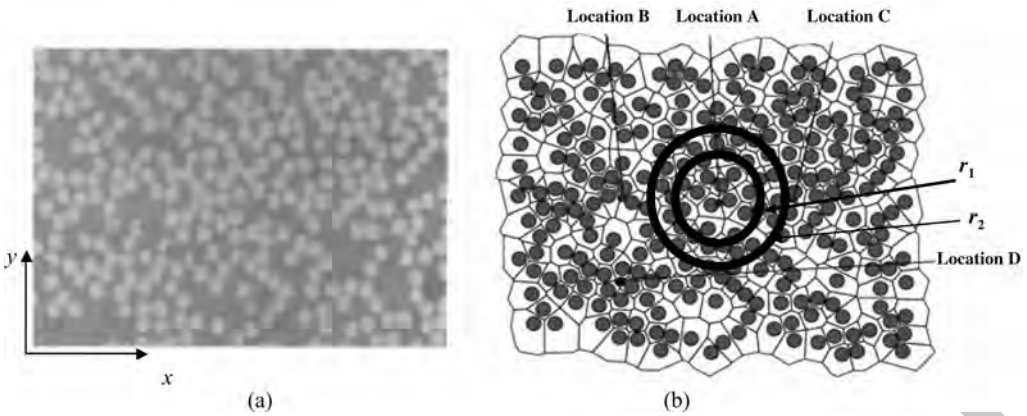

Figure 1. *(a) Optical micrograph of a fiber-reinforced composite microstructure and (b) computer-simulated microstructure tessellated into Voronoi cells.*

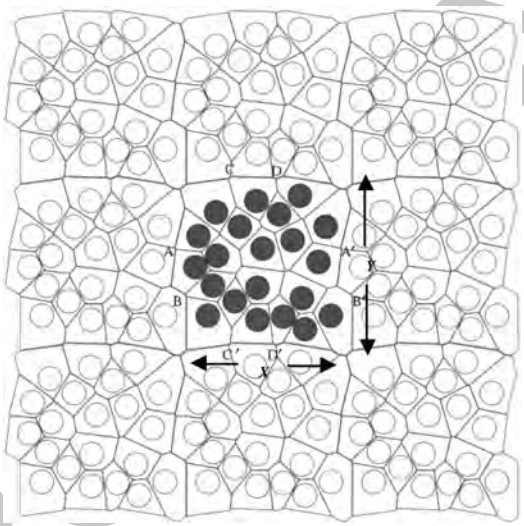

Figure 2. *A local microstructure constructed by periodic repetition of the central statistically equivalent representative volume element (SERVE).*

the boundary of the SERVE with irregular edges as shown in Figure 2. The procedure is discussed later. While the satisfaction of the different criteria may result in nonuniqueness, it is possible to postulate the SERVE as the largest microregion that will satisfy all the above requirements.

Various statistical descriptors have been proposed to characterize and classify microstructures based on the spatial arrangement of the fibers [12–15]. Statistical methods have been used to determine the size scale of the RVE and the number of inclusions contained in it. Pyrz [12] has introduced the pair distribution function, $g(r)$, and the marked correlation function, $M(r)$, to characterize microstructures based on inter-inclusion distances. Shan and Gokhale [16] have derived a RVE window using probability density functions of nearest neighbor distances and stress distribution of

microscopic stresses. Bulsara et al. [17] have used the pair distribution function, $g(r)$, to characterize the microstructural geometry. Apart from these, Zeman and Sejnoha [18] have used the two-point probability function and the second-order intensity function to characterize randomly distributed fibers of a graphite–epoxy composite system. Kanit et al. [19] have provided a quantitative definition for RVE using a combination of statistical and numerical techniques for random composite microstructures. In their study, the RVE size is arrived at by compiling the variances of geometric, elastic, and thermal properties for various microstructural realizations. The statistical distributions of the size, shape, and grain orientations in cubic polycrystals have been used by Ren and Zheng [20] to define the minimum RVE size. Stroeven et al. [21] have quantified the size of the RVE for heterogeneous microstructures by studying the averages and standard deviations of specific factors like particle size, applied peak load, dissipated energy, and strain concentration. These treatments make a strong case for the use of statistical descriptors in the development of the SERVE.

The objective of this two-part article is to review, compare, and demonstrate the effectiveness of various indicators proposed in the literature for the identification of the SERVE for real nonuniform and nonperiodic composites. It may be assumed, at least as a first-order approximation, that the SERVE will suffice to represent the effective moduli of a microstructural region under nonhomogeneous boundary conditions, e.g., in the multiscale analysis of a unidirectional composite. The first part of this article sequence is restricted to undamaged microstructures with a continuous interface. The second part focuses on microstructures with evolving damage by interfacial debonding, where quantitative descriptors are devised to provide explicit representation of the microstructural damage. The essential difference between the two is that in the first case, the microstructure is essentially fixed and hence one rendering of the SERVE is sufficient. In the latter problem, the microstructure evolution due to damage requires a more complex time/load-dependent treatment for the SERVE.

The micromechanical simulation in this study is conducted by the Voronoi cell finite element model (VCFEM) that has been developed by Ghosh et al. [22–27]. This method is effective in analyzing large microstructural regions with arbitrary dispersions, shapes, and sizes of heterogeneities, as in micrographs of the composite materials (Figure 1(a)). The VCFEM naturally evolves from Dirichlet tessellation of the microstructure to generate a network of multisided Voronoi polygons in two dimensions (Figure 1(b)). Each Voronoi cell with its embedded heterogeneities (particle, fiber, void, crack, etc.) may be interpreted as the neighborhood of that heterogeneity and is treated as a single finite element. By combining assumed stress hybrid finite element formulations with essential characteristics of micromechanics, a high level of computational efficiency with good accuracy and resolution has been achieved with this method. The VCFEM has been successful in significantly reducing computational degrees of freedom and current VCFEM computing effort is estimated to be $\approx$60–70 times lower than most conventional FEM packages for modeling complex microstructures.

METHODS TO ESTIMATE STATISTICALLY EQUIVALENT REPRESENTATIVE VOLUME ELEMENTS

Arriving at the optimal SERVE size is important to prevent erroneous estimation of effective properties with smaller representative domains, or requiring huge computational

resources with larger domains. To achieve this objective for undamaged fiber-reinforced microstructures, a few measures involving geometric and mechanical properties are examined to estimate the SERVE satisfying criteria (i–iii) mentioned in the introduction. The different methods used in this task are discussed next.

Convergence of the Effective Elastic Stiffness Tensor

The domains for which the effective homogenized stiffness tensor $[E^{\mathrm{H}}_{ijkl}]$ converges to that for the entire microstructure, at least locally, is an important metric in the estimation of the SERVE. For a given heterogeneous microstructure, the stiffness tensor $[E^{\mathrm{H}}_{ijkl}]$ may be evaluated by volume averaging the microscopic stresses, $[\sigma^{kl}_{ij}]$ generated by applying displacement boundary condition corresponding to a unit macroscopic strain and using the expression (see [28]):

$$\left[E^{\mathrm{H}}_{ijkl}\right] = \langle \sigma^{kl}_{ij} \rangle_Y = \frac{1}{|Y|}\int_Y \sigma^{kl}_{ij}\,\mathrm{d}Y \tag{1}$$

where $[E^{\mathrm{H}}_{ijkl}]$ is the effective stiffness tensor, Y is the microstructural volume element, and σ^{kl}_{ij} corresponds to the microscopic stress developed as a consequence of the applied macroscopic strain of $\bar{\varepsilon}_{kl}$. The boundaries of the domain are subjected to periodic conditions, which are explained next.

The problems considered in this article are for unidirectional fiber-reinforced composite microstructures and plane strain conditions are assumed. Consequently, the components of $[E^{\mathrm{H}}_{ijkl}]$ are calculated from the solutions of three separate boundary value problems of the microstructural element, corresponding to:

(i) macroscopic normal strain field

$$\begin{Bmatrix} \bar{\varepsilon}_{xx} \\ \bar{\varepsilon}_{yy} \\ \bar{\varepsilon}_{xy} \end{Bmatrix}^{\mathrm{I}} = \begin{Bmatrix} 1 \\ 0 \\ 0 \end{Bmatrix};$$

(ii) macroscopic normal strain field

$$\begin{Bmatrix} \bar{\varepsilon}_{xx} \\ \bar{\varepsilon}_{yy} \\ \bar{\varepsilon}_{xy} \end{Bmatrix}^{\mathrm{II}} = \begin{Bmatrix} 0 \\ 1 \\ 0 \end{Bmatrix};$$

and

(iii) macroscopic shear strain field

$$\begin{Bmatrix} \bar{\varepsilon}_{xx} \\ \bar{\varepsilon}_{yy} \\ \bar{\varepsilon}_{xy} \end{Bmatrix}^{\mathrm{III}} = \begin{Bmatrix} 0 \\ 0 \\ 1 \end{Bmatrix}.$$

The strain in the fiber direction is set to zero, i.e., $\bar{\varepsilon}_{zz} = 0$ for all these problems. In VCFEM analysis for the microstructural stresses, the macroscopic unit strains are applied as body forces on the microstructural domain being analyzed, as discussed in [28,29]. In addition, periodic conditions are imposed on the boundary of the two-dimensional microstructural domain, thus constraining points on the boundary to displace periodically. For VCFEM nodes on the boundary, separated by periods X, Y (Figure 2) along one or more coordinate directions, the displacement constraints are expressed as:

$$u_i(x, y) = u_i(x \pm k_1 X,\ y \pm k_2 Y), \quad i = 1, 2 \tag{2}$$

where k_1, k_2 may assume values 0 or 1, depending on the node locations. A special method of constructing a periodic computational domain with non-straight edges containing periodically positioned nodes for the nonuniform microstructure has been developed in [29,30]. The essential steps in this construction are:

(i) The local microstructure consisting of a set of nonuniform inclusions that constitute the local RVE is identified.
(ii) The RVE is subsequently repeated in the x- and y-directions for a few period lengths as shown in Figure 2. In this task, for every fiber in the original RVE at a location (x, y), repetitive fibers are placed at $(x \pm k_1 X, y)$, $(x, y \pm k_2 Y)$, and $(x \pm k_1 X, y \pm k_2 Y)$, where k_1 and k_2 are integers and X and Y are periods in the x- and y-directions. The period lengths X and Y are selected such that the fiber area fraction of the RVE is nearly the same as that of the local microstructure.
(iii) The extended domain of multiply repeated RVEs is then tessellated into a network of Voronoi cells using techniques developed in [27] as shown in Figure 2. The boundary of the central RVE is generated as the aggregate of the outside edges of all the Voronoi cells associated with the fibers near the boundary. The resulting RVE has irregular edges due to the nonuniform arrangement of the fibers. The corresponding nodes on the RVE boundary are periodic, i.e., for every boundary node, a periodic pair can be identified on the boundary at a distance of one period along one or both of the coordinate directions (AA′, BB′, CC′, and DD′ in Figure 2). Periodicity constraint conditions are then imposed on the nodal displacements following Equation (2).

In 2D plane problems, nine components of the homogenized stiffness tensor $[E^{\mathrm{H}}_{ijkl}]$ are evaluated using Equation (1) for each applied macroscopic strain field. The contracted notations are used to represent $[E^{\mathrm{H}}_{ijkl}]$ in terms of the stiffness tensor $[E^{\mathrm{H}}_{ij}]$ as:

$$\begin{pmatrix} E_{11} & E_{12} & E_{13} \\ E_{21} & E_{22} & E_{23} \\ E_{31} & E_{32} & E_{33} \end{pmatrix} \underset{\longleftarrow}{\longrightarrow} \begin{pmatrix} E_{1111} & E_{1122} & E_{1112} \\ E_{2211} & E_{2222} & E_{2212} \\ E_{1211} & E_{1222} & E_{1212} \end{pmatrix}$$

At a given location in the micrograph, a sequence of RVE windows of different sizes is constructed by incrementally increasing the number of fibers included. The phase volume fraction in each of the windows is chosen to match the volume fraction of the overall microstructure to within a prescribed tolerance. For each window, components of the

effective stiffness tensor are evaluated and convergence is established through a comparison of the Frobenius norm of the effective homogenized stiffness tensor,

$$\| E^{\mathrm{H}} \| = \sqrt{\sum_{i=1}^{3}\sum_{j=1}^{3}\left(E_{ij}^{\mathrm{H}}\right)^2} \tag{3}$$

The SERVE is taken to be the smallest window for which the difference in the individual components as well as in the norm satisfy the criteria

$$\frac{\| E_{ij}^{\mathrm{H}} \|^{\mathrm{micrograph}} - \| E_{ij}^{\mathrm{H}} \|^{\mathrm{RVE}}}{\| E_{ij}^{\mathrm{H}} \|^{\mathrm{micrograph}}} \leq \mathrm{TOL} \qquad \frac{\| E^{\mathrm{H}} \|^{\mathrm{micrograph}} - \| E^{\mathrm{H}} \|^{\mathrm{RVE}}}{\| E^{\mathrm{H}} \|^{\mathrm{micrograph}}} \leq \mathrm{TOL} \tag{4}$$

The superscript micrograph corresponds to the entire local micrograph that is available. A tolerance of TOL = 5% is taken in this study. Finally, it is important to examine whether the SERVE selected is location independent. The SERVE is constructed by the above-mentioned procedure for a number of randomly chosen locations in the overall microstructure. The window that satisfies the required characteristics for SERVE can be considered as the SERVE for the local microstructure.

Statistical Functions of Microstructural Variables

The marked correlation function, $M(r)$, has been introduced by Pyrz [12] for providing a multivariate characterization of the microstructural phase distribution. Marked correlation functions correlate any chosen field variables like stresses, strains, or their dependent functions with the morphology of the microstructure and are expressed as the ratio of state variable and geometric distribution functions as:

$$M(r) = \frac{h(r)}{g(r)} \tag{5a}$$

A declining value of $M(r)$ indicates reduced correlation between elements of the microstructure. It is thus a good metric for the estimation of the SERVE, which may be interpreted as the region of influence. The state variable dependent function $h(r)$ is derived from the mark intensity function, $H(r)$, as:

$$h(r) = \frac{1}{2\pi r}\frac{\mathrm{d}H(r)}{\mathrm{d}r} \qquad \text{where } H(r) = \frac{1}{m^2}\frac{A}{N^2}\sum_{i}^{N}\sum_{j=1}^{j_i} m_i m_j(r) \tag{5b}$$

Here m_i represents a 'mark' associated with the ith fiber, where a 'mark' can be any chosen state variable field in the microstructure that is considered significant for the problem considered with respect to the effective size of the SERVE. For observations within a finite window of area A, the variable r is a measure of the radial distance of influence and $m_j(r)$ corresponds to the mark associated with the jth fiber at a radial distance r. In Equation (5b), m is the mean of all marks, N is the total number of fibers, and j_i is the number of fibers that have their center within a circle of radius r centered at the ith fiber.

The pair distribution function, $g(r)$, corresponds to the probability, $g(r)\,\mathrm{d}r$, of finding an additional fiber center between the concentric ring of radii r and $r+\mathrm{d}r$, respectively. It characterizes the occurrence intensity of interfiber distances and is expressed as:

$$g(r) = \frac{1}{2\pi r}\frac{\mathrm{d}K(r)}{\mathrm{d}r} \qquad \text{where } K(r) = \frac{A}{N^2}\sum_{k=1}^{N} I_k(r) \tag{6}$$

where $I_k(r)$ is the number of additional fiber centers that lie inside a circle of radius r about an arbitrarily chosen fiber. Here, $K(r)$ is a second-order intensity function defined in [13] as the number of additional fibers that lie within a distance r of a fiber center and divided by the number density N/A of fibers. With increasing r values, circles about fibers that are near the edges of a finite-sized window may extend outside the observation window and appropriate correction factors have been proposed in [12–15] to account for the edge effects in the evaluation of $K(r)$. These correction factors pose restrictions on the maximum size r that can be chosen and may lead to overestimation of $K(r)$. The following steps are needed to evaluate a SERVE size using $M(r)$ for a nonuniform microstructure:

(i) Calculate $K(r)$ from Equation (6) by constructing circles of radius r about all the fibers and counting the additional number of fibers lying inside these circles. A different approach than that in [12–14] is introduced here to account for the edge effects. The local microstructure is repeated periodically in both the x- and y-directions for several period lengths. For the fibers near the edge of the window, the circle of radius r can extend outside the window and include fibers from the surrounding extended microstructure.

(ii) Determine $g(r)$ from the values of $K(r)$. Plot the distribution of $g(r)$ as a function of r for the microstructure. For a statistically random distribution, the pair distribution function approaches unity at large radial distances.

(iii) Identify the radius of convergence r_0 from the $g(r)$ plot for which $g(r) \approx 1$ for $r > r_0$. Local minor undulations due to the finite size of the fibers may be smeared out for $r > r_0$. An initial estimate for the SERVE is made from the radial distance r_0.

(iv) Assign an appropriate microstructural variable field associated with each fiber as a 'mark'. Commonly assumed marks are principal stresses and strains, Von Mises stress, interfacial traction at the fiber–matrix interface, etc.

(v) Evaluate the marked correlation function, $M(r)$, using Equation (5). $M(r) = 1$ corresponds to a regular distribution of circular heterogeneities having identical marks. Values of $M(r) > 1$ indicate positive correlation, while values of $M(r) < 1$ indicate repulsion between marks. For nonuniform microstructures, $M(r)$ stabilizes to near-unit values at a radius of convergence r_p, such that for $r > r_p$, $M(r) \approx 1$ and the local morphology ceases to have significant influence on the state variables. Hence, the radius r_p corresponds to the scale of the local correlation between physical behavior and the microstructure morphology and provides an estimate for the SERVE size.

MARKED CORRELATION FUNCTION WITH GEOMETRIC PARAMETER-BASED MARKS

While the traction-based marks are found to yield satisfactory estimates of the SERVE, it is of interest to see if similar results can be generated by using marks that are purely

geometric parameters. A weighted function of geometric parameters has been constructed in [22] to predict the initiation of debonding in the microstructure. A similar function is constructed in this study as a mark to represent geometric parameters, which contribute to the initiation of damage. The mark associated with the kth fiber is defined as:

$$m_k = w_1 S_1^k + w_2 S_2^k + w_3 S_3^k \tag{7}$$

where S_i^k are geometric parameters characterizing the local distribution of inclusions and w_i are weight that can be determined from inverse analysis. In Equation (7), S_1^k is a measure of the normalized local area fraction for the kth fiber defined as:

$$S_1^k = \frac{(\mathrm{LAF})^k}{\max\limits_{1 \le j \le N} (\mathrm{LAF})^j} \tag{8}$$

where N is the total number of fibers and $(\mathrm{LAF})^j$ is the local area fraction for the jth fiber. The area fraction is evaluated as the ratio of the fiber cross-sectional area to the area of the respective Voronoi cell [14,27]. The normalized measure of the inverse of the near-neighbor distance for the kth fiber is defined as:

$$S_2^k = \frac{(\mathrm{IND})^k}{\max\limits_{1 \le j \le N} (\mathrm{IND})^j} \tag{9}$$

where $(\mathrm{IND})^j$ is the inverse of the near-neighbor distance of the jth fiber. The near neighbors of a given fiber are those that share common edges of the Voronoi cell. The near-neighbor distance is the average of the distances between an inclusion and its neighboring inclusions. Finally, S_3^k is a normalized measure of the number of near neighbors for the kth fiber

$$S_3^k = \frac{(\mathrm{NN})^k}{\max\limits_{1 \le j \le N} (\mathrm{NN})^j} \tag{10}$$

where $(\mathrm{NN})^j$ is the number of near neighbors for the jth fiber. The number of near neighbors is the count of the number of neighboring Voronoi cells for a given Voronoi cell.

COEFFICIENT OF VARIATION OF THE AREA FRACTION

In continuation with metrics based on pure geometrical parameters of the microstructure, a procedure for microstructure characterization, introduced in [31], involving the variability of the one-point correlation function i.e., the area fraction, is also examined. Consistent with [31], the evaluation of a homogenized length scale (d_{H}) for a nonuniform microstructure is carried out using the following steps:

(i) Repeat the representative microstructure periodically in the x- and y-directions to arrive at a suitable large value for the reference dimension length, L_{d}.
(ii) Divide the domain of length, L_{d}, into a number of small square areas of dimension d.
(iii) Evaluate the area fractions within each of these square areas. The coefficient of variation, defined as the ratio of the standard deviation of the area fractions, σ_{af}, to the mean area fraction of the domain, A_{af}, is evaluated for each length-scale d of the square area.

(iv) Steps (ii) and (iii) are repeated with each increasing square tile of size d.
(v) Evaluate the coefficient of variation (COV) using the expression [31]:

$$\mathrm{COV} = \frac{\sigma_{\mathrm{af}}}{A_{\mathrm{af}}} = \left(\frac{\pi}{4A_{\mathrm{af}}}\right)^{0.5}\left(\frac{d}{L_{\mathrm{d}}}\right)^{-1} \tag{11}$$

where (d/L_{d}) is the normalized square size. From Equation (11), the logarithmic plot of the COV and normalized square size is linear. A plot of $\sigma_{\mathrm{af}}/A_{\mathrm{af}}$ versus (d/L_{d}) is created for different values of d in the logarithmic scale.
(vi) The size of the square tile d is evaluated from the intercept of the plot with a line parallel to the horizontal axis (d/L_{d}), corresponding to the prescribed tolerance. This value corresponds to the homogeneous scale length (d_{H}) for the microstructure.

Distribution of Critical Microstructural Variables

Distribution functions of critical microstructural variables have been compared for candidate RVEs with those for the entire microstructure to estimate the size of RVEs in nonuniform microstructures by Shan and Gokhale in [16]. The method is a variant of the method described in the section on 'convergence of the effective elastic stiffness tensor', in that the SERVE criterion based on effective moduli is replaced by the distribution of critical microscopic variables. Since traction at the fiber–matrix interface is a precursor to interfacial debonding, it is considered as a critical variable in the estimation of SERVE in this article. Similar to what has already described, the procedure entails the following steps:

(i) Extract volume elements of increasing sizes from the material micrograph with the phase volume fractions in each microstructural element matching that of the entire microstructure to within a prescribed tolerance.
(ii) The microstructural volume elements are subjected to periodicity boundary constraints and loaded with a macroscopic uniaxial unit strain as already described and the boundary value problem is analyzed by the VCFEM. Subsequently, the extent of the interface that is likely to undergo debonding is analyzed for each fiber. A critical traction value, T_{c}, above which the interface can debond, is prescribed for this task. The lengths of segments on all the interfaces where $T \geq T_{\mathrm{c}}$ are computed and summed up for the total interface length, l_{tc}, with traction greater than T_{c}. The ratio of the length l_{tc} with high traction to the total length of all the interfaces in the microstructural element, l_{me}, is defined as the critical interfacial fraction $\mathrm{CIF} = l_{\mathrm{tc}}/l_{\mathrm{me}}$. For each microstructural element, the CIF is evaluated for a range of the critical traction value, T_{c}, and the distribution is plotted as a function of T_{c}. The distribution functions are constructed for microstructural element of increasing size and compared with that for the entire microstructure. The smallest element for which the distribution matches that for the entire microstructure to within a prescribed tolerance provides an estimate for the SERVE.
(iii) Repeat Step (ii) for different loading directions and estimate the optimal SERVE.
(iv) Verify if the SERVE is location dependent by repeating Steps (i) through (iii) for different locations in the microstructure. The largest SERVE that satisfies the required conditions is taken as the optimal SERVE.

Two-point Correlation Functions for Measure of Anisotropy

Directionality in the microstructure is of relevance in the determination of the RVE. An isotropic microstructure allows the use of radial distribution functions for spatial characterization, while anisotropy necessitates satisfying the condition that the SERVE is independent of the loading direction. For determining morphological characteristics and the directional properties, the two-point probability function discussed in Torquato [32] and Saheli et al. [33], is implemented. For multiphase microstructure, the two-point probability function is defined as the probability that two points at positions x_1 and x_2, separated by a distance r are found in the phase i. It is expressed as:

$$P_{ij}(r) = P\left\{I^{(i)}(x_1) = 1,\ I^{(j)}(x_2) = 1\right\} \tag{12}$$

where $I^{(i)}(x)$ is the indicator function for the ith phase that has two possible values 0 or 1 for a fixed x. The function $P_{22}(r)$ corresponds to the probability that two points separated by a distance $|r = x_2 - x_1|$ at a given orientation are in the fiber phase, is examined in this study for microstructural anisotropy. For a statistically homogeneous and isotropic microstructure, $P_{22}(r)$ follows two properties, namely: (i) $P_{22}(0) = \mathrm{AF}$ at $r = 0$ and (ii) $\lim_{r\to\infty} P_{22}(r) = \mathrm{AF}^2$ or the square of the area fraction in the limit.

The following steps are undertaken for evaluating $P_{22}(r)$:

(i) The micrograph is periodically repeated in both the x- and y-directions for several period lengths.
(ii) In a given period, for a fixed angle of orientation θ, evaluate $P_{22}(r)$ for two points separated by r.
(iii) Increase the separation distance r in increments of Δr and repeat Step (ii).
(iv) Change the orientation angle, θ, and repeat Steps (ii) and (iii). Plots of $P_{22}(r)$ versus r for different orientations characterize directional properties in the microstructure.

In the next section, methodologies for evaluating the SERVE are examined for a composite micrograph.

EVALUATING THE SERVE FOR A REAL COMPOSITE MICROGRAPH

Figure 1 shows a $100 \times 79.09\,\mu\mathrm{m}^2$ optical micrograph of a steel fiber-reinforced polymer matrix composite that is analyzed in this study. Fibers in the microstructure are aligned perpendicular to the plane of the paper and all the fibers have circular cross sections with a radius of 1.75 μm. Figure 1(b) shows a computer-generated image of the optical micrograph that is tessellated into a network of Voronoi cells based on algorithms presented in [27]. The nonsmooth boundary is a consequence of tessellating the domain with a periodic boundary. It is apparent that the arrangement of fibers is nonuniform with regions of fiber clusters. The matrix material is an epoxy with Young's modulus, $E_\mathrm{m} = 4.6\,\mathrm{GPa}$ and Poisson's ratio, $\nu_\mathrm{m} = 0.4$. The steel fiber material has Young's modulus, $E_\mathrm{f} = 210\,\mathrm{GPa}$ and Poisson's ratio, $\nu_\mathrm{f} = 0.3$. The fiber–matrix interface is assumed to be continuous and a 2D plane strain assumption ($\varepsilon_{zz} = 0, \varepsilon_{xz} = 0, \varepsilon_{yz} = 0$) is made in the solution. Methodologies described in the previous section using the VC FEM for micromechanical analysis, are now applied to the microstructure to evaluate the size of the SERVE.

SERVE from Effective Elastic Stiffness Tensor

Figure 3(a)–(g) illustrates windows of different sizes with periodic boundaries. The windows are chosen from the center of the microstructure for evaluating the effective stiffness tensor following steps outlined in the subsection of 'Methods to Estimate SERVE'. The smallest window size of $\approx$10 μm contains 10 fibers, while the largest 63 μm window contains 150 fibers. Here, the term 'size' refers to the diameter of a circle containing the necessary inclusions, from which the window with periodic boundary is generated. Windows of sizes 22 μm (20 fibers) and 29 μm (33 fibers) are created from concentric circles of radius r_1 and r_2, respectively in Figure 1(b). Table 1 lists the area fractions of the various periodic windows generated and compares them with that of the

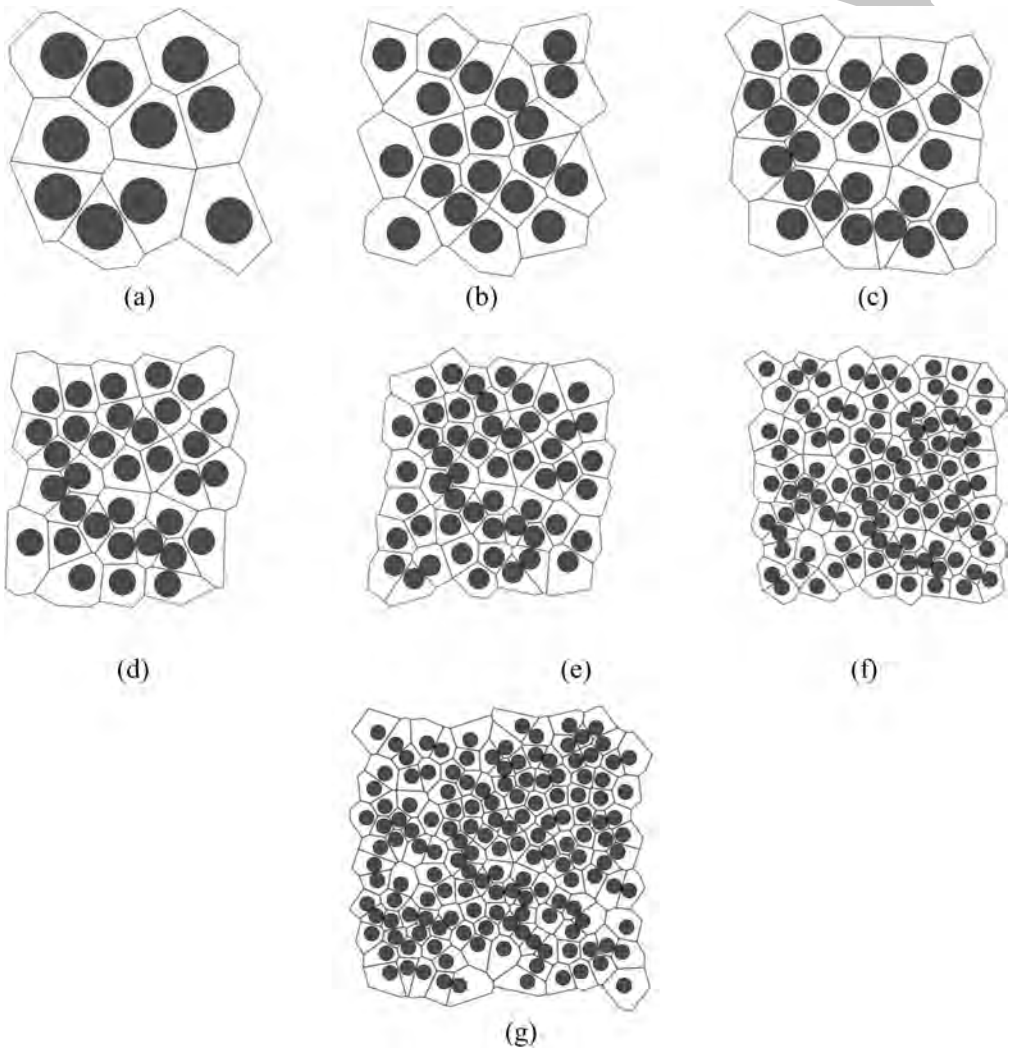

Figure 3. *Microstructural elements of radius: (a) 15 μm containing 10 fibers; (b) 22 μm containing 20 fibers; (c) 25 μm containing 25 fibers; (d) 29 μm containing 33 fibers; (e) 35 μm containing 52 fibers; (f) 52 μm containing 102 fibers; and (g) 63 μm containing 151 fibers.*

Table 1. Area fraction of RVEs with increasing number of fibers in the RVE.

Window size	5 μm	10 μm	15 μm	22 μm	25 μm	29 μm	35 μm	52 μm	63 μm	Micrograph
Number of fibers	1	5	10	20	25	35	50	100	150	264
Area fraction (%)	32.9	31.21	31.50	32.06	32.16	31.52	33.14	32.28	31.32	32.315

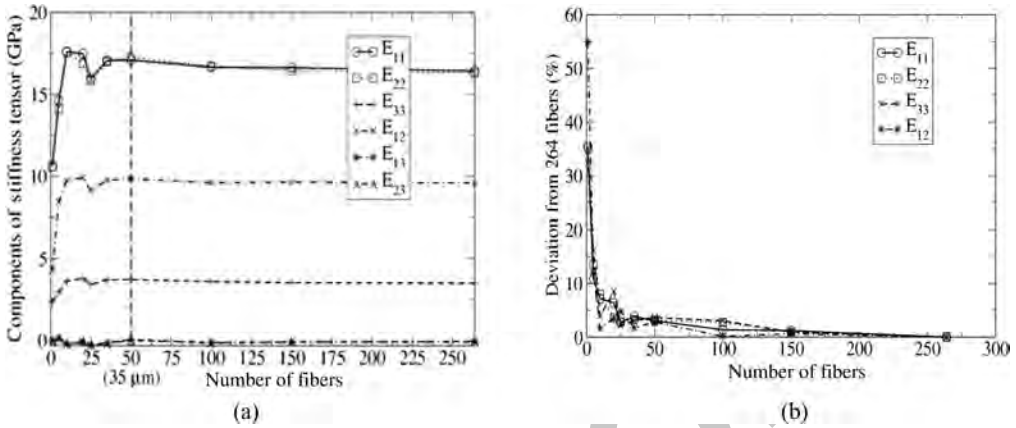

Figure 4. *Plots showing (a) convergence of the stiffness tensor components and (b) deviation of the stiffness tensor from that of the micrograph, at location A.*

entire micrograph. The convergence of various components of the effective stiffness tensor with increasing window size at a location A in Figure 1(b) is depicted in Figure 4(a). Figure 4(b) shows the deviation of these components for each window from those for the entire micrograph. The single fiber window shows a 55% deviation for E_{11}, E_{22}, and 32% for E_{33}. For all the locations considered, windows containing 52 or more fibers always exhibit a <3% deviation for the stiffness components. The convergence in the Frobenius norm of the stiffness $\|E^{\mathrm{H}}\|$ in Equation (3) and the corresponding deviations at three different locations are shown in Figure 5(a) and (b). The windows containing 52 or more fibers exhibit a <2% deviation from the stiffness of the entire micrograph. A region of radius 35 μm, encompassing 52 fibers is found to exhibit stabilized stiffness components and is also found to be independent of location in the microstructure. From the requirements outlined in the criteria (i), (ii), and (iv) of the introduction, this can be regarded as a candidate SERVE of the microstructure.

SERVE from Marked Correlation Functions

Figure 6 compares $g(r)$ for a Poisson distribution of points ($g(r) = 1$) with those for the micrograph where the edge effect is accounted for by both alternative methods mentioned. At lower values of r, there is a significant deviation from the unit value due to short-range geometric disorders like clustering. Convergence is assumed, if the percentage change in incremental area under each $g(r)$ or $M(r)$ curve is measured to be below a predetermined tolerance of 5%. The function $g(r)$ converges to unity with increasing values of r (>15 μm) containing about 35 fibers. It is observed that the periodic repetition method works better

than the circumference ratio factor method with respect to the convergence to unity. Since the Poisson distribution does not strictly apply for a random distribution of fibers, the $g(r)$ for micrograph has also been compared with a hard core (HC) distribution of fibers (Figure 6). The HC distribution is generated as a variant of the Poisson distribution with the imposition of the constraints that inclusions are not allowed to overlap and all the inclusions are completely contained within the region. From Figure 6, it can be observed that the micrograph depicts the same trend as a HC model for $g(r)$ distribution. Thus, the distribution of fibers in the micrograph is essentially random in nature.

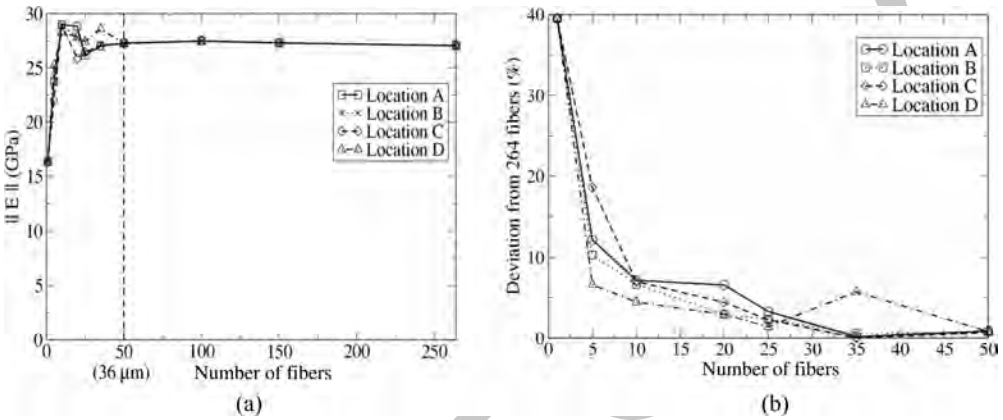

Figure 5. *Plots showing (a) convergence of $\|E^H\|$ for windows of increasing sizes and (b) deviation of $\|E^H\|$ from that of the entire micrograph, at different locations.*

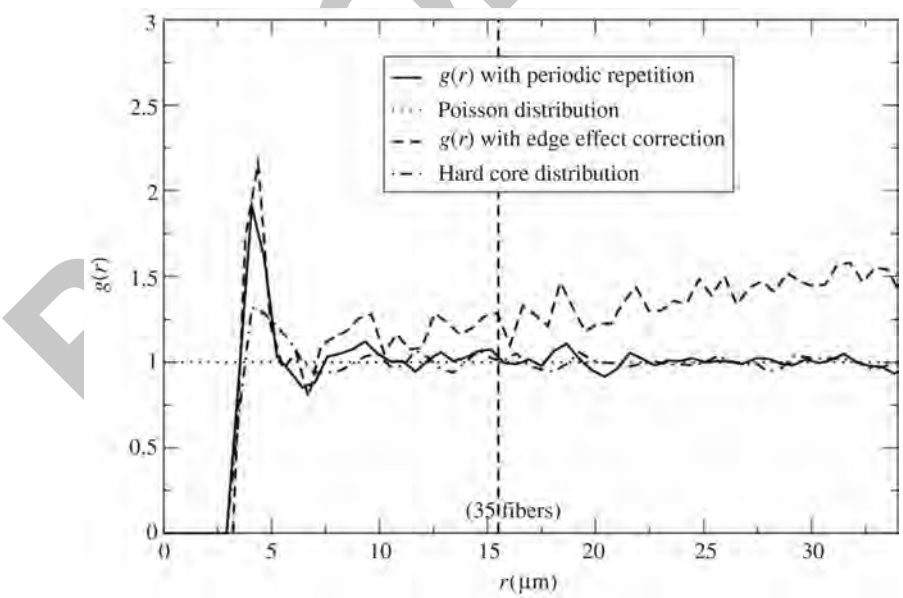

Figure 6. *Plots of the pair distribution function, g(r), with two methods of edge correction, compared with that for a Poisson's distribution.*

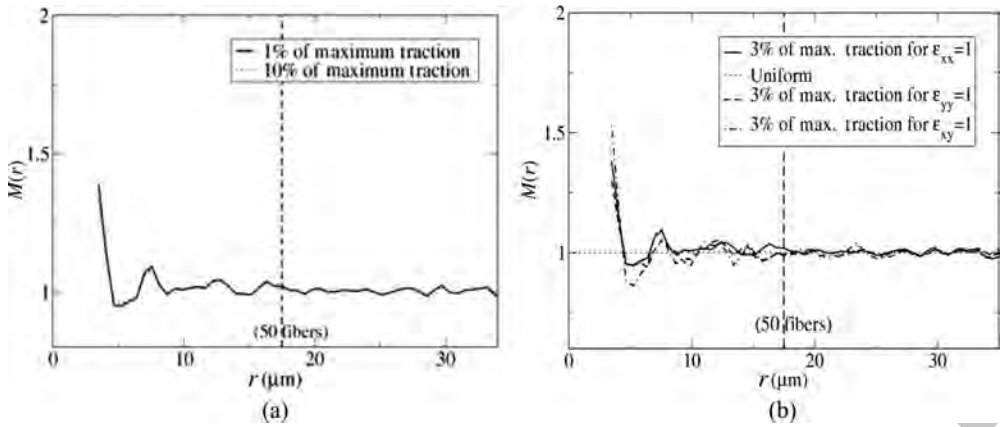

Figure 7. *Comparison of M(r) for (a) average traction of 1 and 10% of points experiencing maximum traction, and (b) for applied unit macroscopic normal and shear strains.*

The maximum traction at the fiber–matrix interface is a good indicator of interfacial debonding initiation, which will be considered in the second part of this article. Hence this is considered as a candidate mark in the evaluation of $M(r)$. Traction is evaluated as the resultant of the normal and tangential components of traction given as, $\sqrt{T_n^2 + T_t^2}$, where T_n is a tensile traction. The mark is not taken as the traction at a single point on the interface. Instead, it is taken as the average traction of a set of points on the fiber–matrix interface that experience the highest tensile normal components. Figure 7 shows a plot of $M(r)$ versus r for different fractions of points on the interface, under different macroscopic strain conditions. The line $M(r) = 1$ corresponds to a uniform distribution of fibers with identical marks. In Figure 7(a), $M(r)$ is constructed from marks obtained by averaging the tractions of 1 and 10%, respectively, of the points at the fiber–matrix interface that experience the highest traction. The macroscopic strain field for this problem is $\varepsilon_{xx} = 1$, with all other components of $\varepsilon_{ij} = 0$. The two marks result in very similar $M(r)$ distribution and both converge to unity at a radius of convergence $r_p \approx 18\,\mu m$, containing about 50 fibers. Figure 7(b) compares the distribution of $M(r)$ for three different applied uniaxial macroscopic strains $\varepsilon_{xx} = 1, \varepsilon_{yy} = 1$, and $\varepsilon_{xy} = 1$. The mark in this case is the average traction of 3% of the points at the interface. For lower values of radius r, the $M(r)$ plots for the three applied strains do not have the same distribution and show a variation with respect to one another. This is attributed to the directional dependence of the mark values with the applied loading directions. With increasing r values, the local anisotropy in the mark values diminishes and all the three plots converge to depict the same trend for $M(r)$. The radius of convergence for all the cases is $r_p \approx 18\,\mu m$, containing about 50 fibers.

As stated in an earlier section, the values of the weights in Equation (8) have been evaluated in [22] by conducting a sensitivity analysis to arrive at optimal values with respect to the initiation of debonding as: $w_1 = 1.0$, $w_2 = 2.0$, $w_3 = 1.0$. Figure 8 shows a comparison of $M(r)$ obtained from the geometric function with that of the $M(r)$ obtained from maximum traction at the interface. While at lower r values, $M(r)$ for the geometric function is lower, the convergence pattern is similar for both the cases. Both tend towards unity at around $r_p \approx 18\,\mu m$.

From the plots of $g(r)$ and $M(r)$, it can be seen that a window size of approximately twice the radius, i.e., 36 μm, containing ≈50 fibers can be considered as an estimate for the

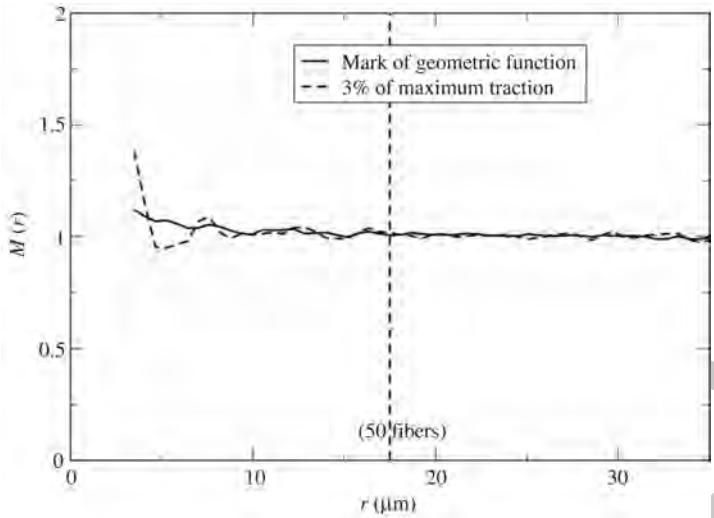

Figure 8. *Comparison of M(r) distribution for marks of geometric function and maximum interfacial traction, respectively.*

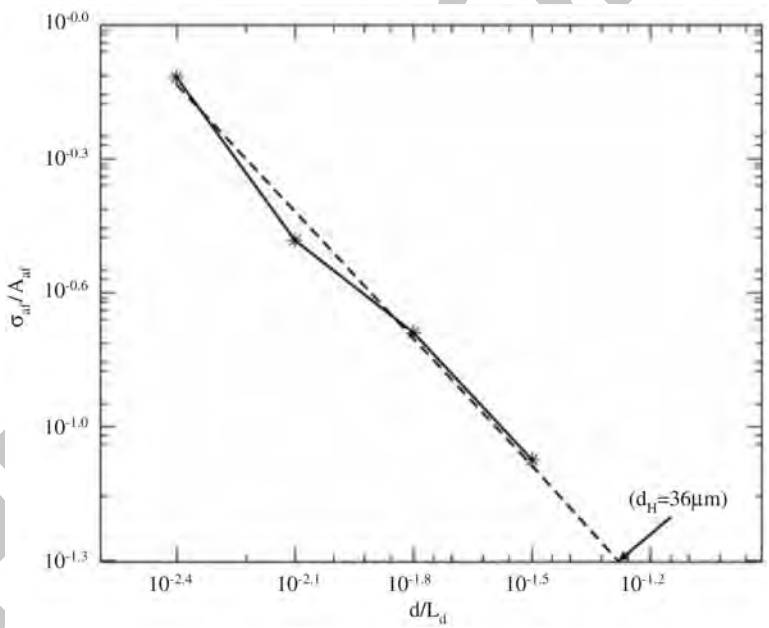

Figure 9. *Coefficient of variation for the micrograph.*

SERVE for this microstructure. This satisfies the criterion (ii) for SERVE mentioned in the introduction.

Finally, for determining the homogenized scale length (d_H) corresponding to the area fraction, a logarithmic plot of σ_{af}/A_{af} versus (d/L_d) is plotted for the micrograph in Figure 9. The dotted line shown in the figure is the linear fit obtained for the plot.

For the given micrograph, with a prescribed tolerance of 5% for COV, the dimension of the homogenized scale length d_H is estimated to be around 36 μm, containing about 50 fibers.

Distribution of Critical Microstructural Variables

Following the steps summarized in the section on distribution of critical microstructural variables, the interfacial tractions are evaluated for windows of increasing sizes by VCFEM as shown in Figure 3(a)–(g). Figure 10(a)–(c) shows the plots of CIF for imposed unit macroscopic strain fields $\varepsilon_{xx} = 1$, $\varepsilon_{yy} = 1$, and $\varepsilon_{xy} = 1$, respectively, for the different window sizes. For $\varepsilon_{xx} = 1$ in Figure 10(a), windows containing at least 35 fibers show a 5% deviation in the CIF distribution from that of the micrograph containing 264 fibers. However, for the other two loading cases in Figure 10(b) and (c), windows containing 52 or more fibers show a close match. Additionally, to ascertain the location

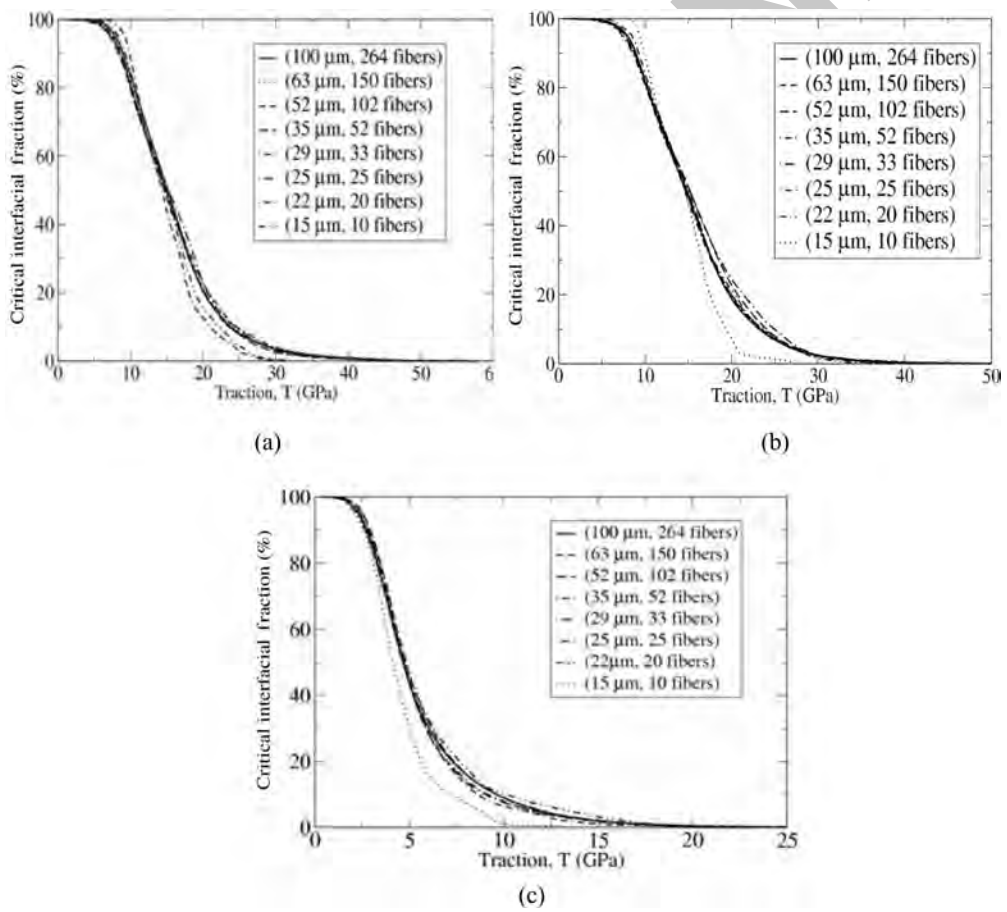

Figure 10. *Critical interfacial fraction ($T \geq T_c$) as a function of the interfacial traction for (a) unit strain $\varepsilon_{xx} = 1$; (b) unit strain $\varepsilon_{yy} = 1$; and (c) unit strain $\varepsilon_{xy} = 1$.*

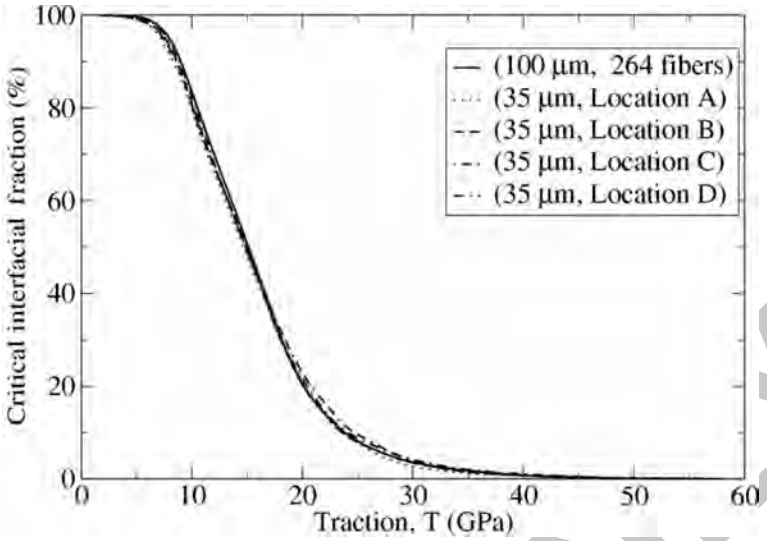

Figure 11. *Comparison of the critical interfacial fraction ($T \geq T_c$) as a function of the interfacial traction at different locations in the micrograph.*

Table 2. Mean and standard deviation of probability density functions of nearest neighbor distance and local area fraction for SERVE (35 μm) at different locations.

	Probability density functions			
	Nearest neighbor distance		Local area fraction	
Location	Mean	Standard deviation	Mean	Standard deviation
Center	6.06	12.26	2.57	2.76
A	6.44	12.71	2.51	2.82
B	5.98	11.89	2.46	2.57
C	5.77	11.53	2.50	2.32

independence of the SERVE, the windows are selected from different locations shown in Figure 1(b). Figure 11 depicts the CIF distribution for windows of size 35 μm containing about 50 fibers, at four locations in the microstructure. The deviation in CIF for the 35 μm window from that for the entire micrograph is <3% for all the loads. To examine if the 35 μm SERVE at different locations are geometrically similar, the probability density functions of the nearest neighbor distance and the local area fraction are calculated at the four different locations and compared in Table 2. The values of mean and standard deviation of the probability density function have little variation, confirming the statistical equivalence of geometry at different locations.

Two-point Correlation Functions for Measure of Anisotropy

Finally, the two-point correlation function $P_{22}(r)$ is plotted for the micrograph in Figure 12. The microstructure does not show any significant variation for $P_{22}(r)$ for the

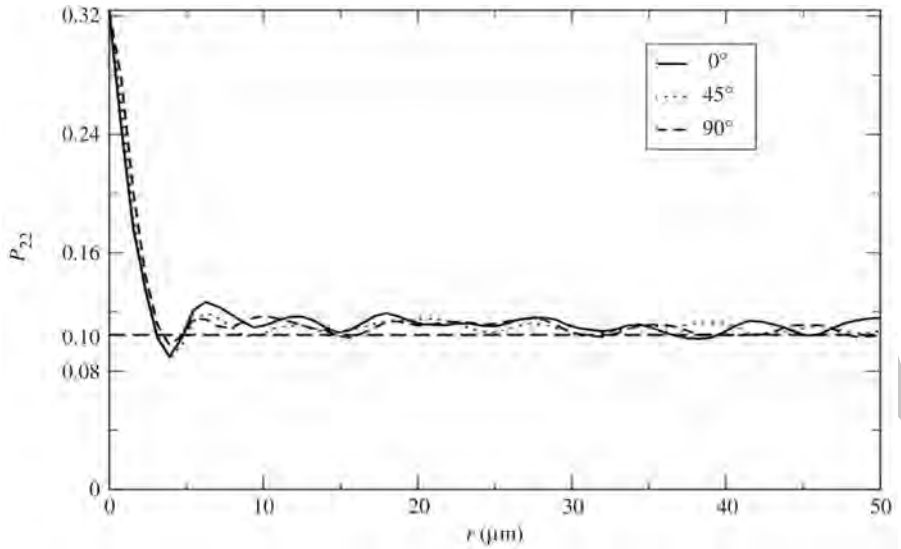

Figure 12. *Two-point statistics as a function of the radial distance for the microstructure.*

various orientations considered, some of which are depicted in the figure. Hence, it is postulated that the microstructure results in isotropic properties due to the near-random or hard core distribution. As discussed in an earlier section, two-point correlation function can be proved to satisfy certain criteria for isotropic materials. At $r = 0$, the value of $P_{22}(r)$ is 0.323 which is equal to the area fraction for the micrograph given in Table 1 (0.32315). With increase in r values, the $P_{22}(r)$ function approaches a value of 0.104, corresponding to the square of the area fraction for the micrograph. The value of $P_{22}(r)$ is 0.109 at $r = 29\,\mu m$, which corresponds to a 5% deviation from the square of the area fraction or $P_{22}(r = \infty)$. However, if the tolerance is set to 9% corresponding to $P_{22}(r) = 0.113$ the radius of influence becomes $r = 18.5\,\mu m$. A slightly higher value of tolerance is needed in this case to match the radius of influence determined by other methods.

DISCUSSION AND CONCLUSIONS

In this first of a two-part article, a number of alternative approaches are proposed to evaluate the size scale of statistically equivalent representative volume elements (SERVEs) for nonuniform microstructures. This article deals with composite microstructures containing elastic matrix and inclusion constituents in the absence of damage. The measures discussed in this article enable the selection of SERVEs that will provide meaningful statistical representation of the entire microstructure with respect to mechanical and geometric properties. A number of alternate criteria is considered in the determination of the scale of the SERVE. These include (a) equivalence of the homogenized stiffness tensor, (b) low influence and correlation of geometric characteristics and state variables beyond its boundaries, (c) agreement in the statistical distribution of the microstructural variables with those for the entire microstructure, (d) equivalence of distributions of local morphological parameters, and (e) independence from loading and location in the microstructure.

Table 3. Method for SERVE estimation and obtained SERVE size.

Method for SERVE estimation	Tolerance (%)	Size of SERVE (μm)	Number of fibers
Convergence of effective elastic stiffness tensor	5	35	50
Marked correlation function	5	36	50
Statistical homogenization of area fraction	5	36	50
Distribution of critical microstructural variables	5	35	50
Two-point correlation function	5	58	135

A micrograph of a unidirectional fiber-reinforced composite is tested for the effectiveness of these criteria in the determination of the SERVE. Various metrics are used in this evaluation. They include convergence of the effective stiffness tensor, marked correlation function of high traction at the fiber–matrix interface, marked correlation function of a weighted geometric function representing the local microstructure, coefficient of variation of the area fraction, the distribution of fraction of the interface that may be on the verge of debonding and the two-point correlation function. A comparison of the estimates for the SERVE size with these metrics is shown in Table 3. For an assumed tolerance, similar size scales of the SERVE are predicted by these alternate methods. This suggests that the different indicators are able to predict similar influence of microstructural elements on one another. In addition, the use of the geometry-based indicators, such as coefficient of variation of area fraction, two-point correlation functions, and mark from geometry point to the fact that for certain problems, the SERVE can be estimated without having to solve the micromechanics problem.

The methods proposed in the study for SERVE estimation also deal with the assessment of anisotropy in the microstructure. A microstructure with anisotropic moduli will be characterized by more than two independent constants, depending on the degree of anisotropy. The two-point correlation function is also an indicator of the nature of microstructural distribution and has been used in determining whether the microstructure is isotropic or anisotropic. The micrograph described in this article shows that the microstructure has isotropic moduli due to its effective elastic stiffness tensor. The micrograph is also found to have an isotropic distribution of fibers from its two-point correlation function. For criteria with the marked correlation function or critical interfacial fraction (CIF) distribution, the condition that SERVE is independent of loading direction can be used to deem isotropy in the microstructure. The SERVE criteria with the marked correlation function and the CIF have been evaluated for three different loading directions and have been satisfied for these three loading cases. From these studies, it is concluded that the microstructure does not exhibit any directional dependence.

For the given micrograph, a window size of 36 μm containing ≈50 fibers is found to possess satisfactory properties of the SERVE. Though the sample micrograph used in this study is somewhat small, the criteria set have been satisfied for this sample. For realistic size 2D composites, the approach will essentially be the same, although a multiscale modeling may be required due to the large number of fibers.

ACKNOWLEDGMENTS

This study has been partially supported by the Air Force Office of Scientific Research through grant No.F49620-98-1-01-93 (Program Director: Dr B. L. Lee) and by the

Army Research Office through grant No. DAAD19-02-1-0428 (Program Director: Dr B. Lamattina). This sponsorship is gratefully acknowledged. Computer support by the Ohio Supercomputer Center through grant PAS813-2 is also gratefully acknowledged.

REFERENCES

1. Hill, R. (1963). Elastic Properties of Reinforced Solids: Some Theoretical Principles, *Jour. Mech. Phys. Solids*, **11**: 357–372.
2. Hashin, Z. and Shtrikman, S. (1963). A Variational Approach to the Theory of the Elastic Behaviour of Multiphase Materials, *Jour. Mech. Phys. Solids*, **11**: 127–140.
3. Hashin, Z. and Shtrikman, S. (1962). On Some Variational Principles in Anisotropic and Nonhomogenous Elasticity, *Jour. Mech. Phys. Solids*, **10**: 335–342.
4. Hashin, Zvi (1962). The Elastic Moduli of Heterogeneous Materials, *Jour. Appl. Mech., Transactions of the ASME*, **29**: 143–150.
5. Jones, Robert M. (1975). *Mechanics of Composite Materials*, Hemisphere Publishing Corporation, USA.
6. Drugan, W.J. and Willis, J.R. (1996). A Micromechanics-based Non Local Constitutive Equation and Estimates of Representative Volume Element Size for Elastic Composites, *Jour. Mech. Phys. Solids*, **44**: 497–524.
7. Willis, J.R. (1982). *Elasticity Theory of Composites, Mechanics of Solids*, The R. Hill 60th Anniversary Volume, pp. 653–686, Pergamon Press, Oxford.
8. Sun, C.T. and Vaidya, R.S. (1996). Prediction of Composite Properties from a Representative Volume Element, *Comp. Sci. Tech.*, **56**: 171–179.
9. Yuan, F.G., Pagano, N.J. and Cai, X. (1997). Elastic Moduli of Brittle Matrix Composites with Interfacial Debonding, *Int. Jour. Solids Struct.*, **34**: 177–201.
10. Boehm, H.J., Rammerstoffer, F.G. and Weissenbek, E. (1993). Some Simple Models for Micromechanical Investigations of Fiber Arrangement Effects in MMC's, *Comput. Mater. Sci.*, **1**: 177–194.
11. Weissenbek, E., Boehm, H.J. and Rammerstoffer, F.G. (1994). Micromechanical Investigations of Arrangement Effects in Particle Reinforced Metal Matrix Composites, *Comput. Mater. Sci.*, **3**: 263–278.
12. Pyrz, R. (1994). Correlation of Microstructure Variability and Local Stress Field in Two Phase Materials, *Mater. Sci. Engng.*, **A177**: 253–259.
13. Pyrz, R. (1994). Quantitative Description of the Microstructure of Composites, Part I, Morphology of Unidirectional Composite Systems, *Comp. Sci. Tech.*, **50**: 197–208.
14. Ghosh, S., Nowak, Z. and Lee, K. (1997). Quantitative Characterization and Modeling of Composite Microstructures by Voronoi Cells, *Acta Mater.*, **45**: 2215–2234.
15. Ghosh, S., Nowak, Z. and Lee, K. (1997). Tessellation-based Computational Methods for the Characterization and Analysis of Heterogeneous Microstructures, *Comp. Sci. Tech.*, **57**: 1187–1210.
16. Shan, Z. and Gokhale, A.M. (2002). Representative Volume Element for Non-uniform Microstructure, *Comput. Mater. Sci.*, **24**: 361–379.
17. Bulsara, V.N., Talreja, R. and Qu, J. (1999). Damage Initiation under Transverse Loading of Unidirectional Composites with Arbitrarily Distributed Fibers, *Comp. Sci. Tech.*, **59**: 673–682.
18. Zeman, J. and Sejnoha, M. (2001). Numerical Evaluation of Effective Elastic Properties of Graphite Fiber Tow Impregnated by Polymer Matrix, *Jour. Mech. Phys. Solids*, **49**: 69–90.
19. Kanit, T., Forest, S., Galliet, I., Mounoury, V. and Jeulin, D. (2003). Determination of the Size of the Representative Volume Element for Random Composites: Statistical and Numerical Approach, *Int. Jour. Solids Struct.*, **40**: 3647–3679.

20. Ren, Z.-Y. and Zheng, Q.-S. (2004). Effects of Grain Sizes, Shapes, and Distribution on Minimum Sizes of Representative Volume Elements of Cubic Polycrystals, *Mech. Mater.*, **36**: 1217–1229.
21. Stroeven, M., Askes, H. and Sluys, L.J. (2004). Numerical Determination of Representative Volumes for Granular Materials, *Comp. Meth. App. Mech. Engng.*, **193**: 3221–3238.
22. Li, S. and Ghosh, S. (2004). Debonding in Composite Microstructures with Morphological Variations, *Int. Jour. Comput. Meth.*, **1**: 121–149.
23. Ghosh, S. and Moorthy, S. Three Dimensional Voronoi Cell Finite Element Model for Modeling Microstructures with Ellipsoidal Heterogeneities, *Comput. Mech.* (in press).
24. Ghosh, S., Ling, Y., Majumdar, B.S. and Kim, R. (2000). Interfacial Debonding in Multiple Fiber-reinforced Composites, *Mech. Mater.*, **32**: 561–591.
25. Moorthy, S. and Ghosh, S. (2000). Adaptivity and Convergence in the Voronoi Cell Finite Element Model for Analyzing Heterogeneous Materials, *Comp. Meth. Appl. Mech. Engin.*, **185**: 37–74.
26. Raghavan, P. and Ghosh, S. (2004). Concurrent Multi-Scale Analysis of Elastic Composites by a Multi-level Computational Model, *Comp. Meth. App. Mech. Engng.*, **193**: 497–538.
27. Ghosh, S. and Mukhopadhyay, S.N. (1991). A Two Dimensional Automatic Mesh Generator for Finite Element Analysis of Random Composites, *Comput. Struct.*, **41**: 245–256.
28. Raghavan, P. and Ghosh, S. (2004). Adaptive Multi-Scale Computational Modeling of Composite Materials, *Comput. Mod. Engng. Sci.*, **5**: 151–170.
29. Ghosh, S., Lee, K. and Raghavan, P. (2001). A Multi-level Computational Model for Multi-scale Damage Analysis in Composite and Porous Materials, *Int. Jour. Solids Struct.*, **38**: 2335–2385.
30. Raghavan, P. and Ghosh, S. (2004). A Continuum Damage Mechanics Model for Unidirectional Composites Undergoing Interfacial Debonding, *Mech. Mater.* (in press).
31. Spowart, J.E., Maruyama, B. and Miracle, D.B. (2001). Multi-scale Characterization of Spatially Heterogeneous Systems: Implications for Discontinuously Reinforced Metal-matrix Composite Microstructures, *Mater. Sci. Engng.*, **307**: 51–66.
32. Torquato, Salvatore (2002). *Random Heterogeneous Materials, Microstructure and Macroscopic Properties*, Springer-Verlag, New York.
33. Saheli, G., Garmestani, H. and Gokhale, A. (2004). Effective Elastic Properties of an Al-SiC Composite using Two-point Statistical Mechanics Approach, In: Ghosh, S., Lee, J.K. and Castro, J. (eds), *Proceedings of 8th International Conference on Numerical Methods in Industrial Forming Processes*, pp. 355–359.